PHYSICAL REVIEW B **91**, 220409(R) (2015)

Achieving large magnetocaloric effects in Co- and Cr-substituted Heusler alloys: Predictions from first-principles and Monte Carlo studies

Vladimir V. Sokolovskiy,[1,2,*] P. Entel,[3] V. D. Buchelnikov,[1] and M. E. Gruner[3]
[1]*Condensed Matter Physics Department, Chelyabinsk State University, 454001 Chelyabinsk, Russia*
[2]*National University of Science and Technology, "MISIS," 119049 Moscow, Russia*
[3]*Faculty of Physics and Center for Nanointegration, CENIDE, University of Duisburg-Essen, D-47048 Duisburg, Germany*
(Received 2 February 2015; revised manuscript received 2 June 2015; published 24 June 2015)

The magnetocaloric properties of Ni-Co-Mn-Cr-In Heusler alloys have been studied by means of *ab initio* calculations and Monte Carlo simulations. We discuss the resulting complex spin configurations, the temperature behavior of entropy, as well as the critical temperatures of the phase transitions. The substitution of 5% Co for Ni and 5% Cr for Mn results in a first-order magnetostructural transition from ferromagnetic austenite to antiferromagnetic martensite, which is accompanied by a spin-flip transition upon cooling. As a result, a large magnetization drop and giant inverse magnetocaloric effect can be achieved of $\Delta T_{ad} \approx 10$ K in a 2 T field across the magnetostructural phase transition.

DOI: 10.1103/PhysRevB.91.220409 PACS number(s): 75.50.−y, 75.10.−b, 75.30.Sg

Ferromagnetic (FM) compounds with a first-order coupled magnetostructural phase transition have attracted interest due to emerging magnetocaloric effects (MCEs) and their possible application in magnetic refrigeration technology [1–4]. Besides the popular materials FeRh [1], $Gd_5(Si_2Gd_2)$ [2,3], and $La(Fe_xSi_{1-x})_{13}$ [4] having comparable cooling power with adiabatic temperature changes of the order of $\Delta T_{ad} \approx -(12–13)$ K, other FM materials having acceptable magnetocaloric properties such as Ni-Mn-(Ga,In,Sn,Sb)-Z (Z = Co, Fe, Cr etc.) Heusler alloys have been widely investigated because of their potential applications as intelligent functional materials [5–16].

Here, we investigate the magnetocaloric properties of a series of (partially different) Heusler alloys in more detail. It is known that the additional element Z can smoothly or sharply change both the magnetic and structural phase transitions. This may bring about a transformation sequence from martensite having low magnetization to a FM austenite with high magnetization, giving rise to better magnetocaloric properties. Our interest in the optimization problem of the MCE in Heusler alloys has been stimulated by recent findings regarding the influence of Co and Cr on the magnetocaloric properties of Ni-Mn-based alloys. A kind of breakthrough regarding Co-doped Ni-Mn-In alloys has been achieved recently by Liu *et al.* [8] observing the giant inverse MCE ($\Delta T_{ad} \approx -6.2$ K) in $Ni_{45}Co_5Mn_{37}In_{13}$ in a magnetic field of 1.9 T and $\Delta T_{ad} \approx -12.8$ K in pulsed fields up to 15 T [16].

Note that, at present, these values of ΔT_{ad} are the highest among all Heusler alloys. For Cr-doped Ni-Mn-(In,Sb), ambiguous results have been recently reported [11–15]. Sharma *et al.* have investigated $Ni_{50}(Mn,2\%Cr)_{34}In_{16}$ by substituting Mn by Cr [11,12], and finding a shift of the martensitic transition temperature T_m from $\approx$ 240 K (0 at. % Cr) to $\approx$ 290 K (2 at. % Cr). The increase of Cr results in the appearance of a paramagnetic (PM) or antiferromagnetic (AFM) gap in the temperature range between T_m and the Curie temperature of martensite T_C^M in low magnetic fields, and below the structural transformation in a lower magnetization. With respect to the inverse MCE, the peak value of ΔS_{mag} increases with increasing Cr [11,12]. Different findings were reported by Sánchez-Alarcos *et al.* [13], who have investigated the effect of a higher amount of Cr on inverse MCEs in $Ni_{50}Mn_{33-x}In_{17}Cr_x$ ($0 \leqslant x \leqslant 4$). It was observed that a Cr-rich second phase appears for all Cr-doped alloys because of the low solubility of Cr in Ni-Mn-In. Thus, the maximum ΔS_{mag} ($\approx$1.4 J/kg K) was found to be six times smaller in a (4 at. % Cr)-doped alloy for a magnetic field change $\Delta H = 6$ T. The authors concluded that the addition of a high amount of Cr to Ni-Mn-In may be highly detrimental to the achievement of a large MCE. A series of Mn-rich $Ni_{50}Mn_{37-x}Cr_xSb_{13}$ Heusler alloys with $0 \leqslant x \leqslant 5$ has been investigated by Khan *et al.* [14,15]. They have suggested that a partial replacement of Mn by Cr results in the destabilization of the martensitic phase due to weakening of the Ni-Mn hybridization. Hence, the Cr substitution is expected to weaken the AFM interactions of the martensitic phase and strengthen the ferromagnetism of $Ni_{50}Mn_{37-x}Cr_xSb_{13}$ alloys, while T_m is found to shift to lower temperatures with increasing Cr.

In order to resolve this contradiction and to optimize the MCE in these alloys, we have undertaken theoretical investigations by means of *ab initio* calculations and Monte Carlo (MC) simulations of Co- and Cr-doped $Ni_{50}Mn_{37}In_{13}$ alloys with a substitution of 5 at. % Co for Ni and 5 at. % Cr for Ni, Mn, or In. We have extended our microscopic model to include random magnetic clusters and long-range exchange interactions between all magnetic atoms, which are taken from *ab initio* calculations. The total Hamiltonian $\mathcal{H}$ consists of magnetic ($\mathcal{H}_{mag}$), elastic ($\mathcal{H}_{el}$), and magnetoelastic ($\mathcal{H}_{int}$) parts:

$$\mathcal{H} = \mathcal{H}_{mag} + \mathcal{H}_{el} + \mathcal{H}_{int}, \quad (1)$$

which are described by the q-state Potts and three-state Blume-Emery-Griffiths (BEG) models. Full information on the Hamiltonian allowing to describe the martensite-austenite transformation with thermal hysteresis and MCE can be found in Refs. [17–19].

Three subsequent steps have been used in the *ab initio* computation. First, we determined the equilibrium

*vsokolovsky84@mail.ru

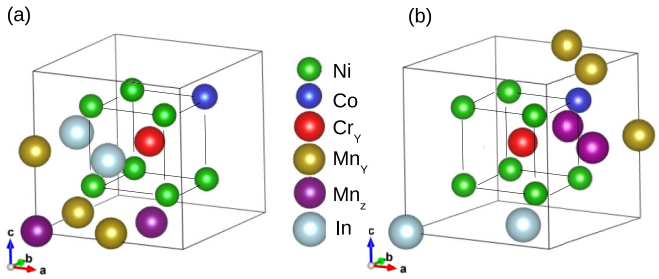

FIG. 1. (Color online) (a), (b) Two types of 16-atom supercells for $Ni_7Co_1Mn_5Cr_1In_2$ were used.

lattice parameters and spin configurations (reference states) of the materials using the VASP [20] and the QUANTUM ESPRESSO (QE) [21] packages. The energy calculations with tetragonal distortion c/a were performed for the 16-atom supercell $Ni_7Co_1Mn_5Cr_1In_2$ ($Ni_{43.75}Co_{6.25}Mn_{31.25}Cr_{6.25}In_{12.5}$) being close in composition to $Ni_{45}Co_5Mn_{37}In_{13}$ which exhibits a large ΔT_{ad} [8,16]. We considered two kinds of supercells with different distributions of $Mn_{Y(Z)}$ and In atoms [17], while in each cell Ni, Co, and Cr atoms are fixed [see Figs. 1(a) and 1(b)]. Here, Mn_Y and Mn_Z refer to Mn located on the original Mn sites and on the Z (In) sites, respectively. Note that Co and Cr substitute here for Ni and Mn_Y, respectively. For both kinds of supercells, Cr has three nearest neighbors (NN) Mn_Y. Regarding Mn_Z, it is obvious that in the case of supercell No. 1 [Fig. 1(a)], Cr has one NN Mn_Z, while in the case of supercell No. 2 [Fig. 1(b)], it has two NN Mn_Z. Such a difference in the atomic distribution may lead to different magnetic exchange interactions. It should be pointed out that there are only these two different possibilities of distributing Mn_Z, which are shown in Fig. 1, and other distributions will be equivalent to these.

The calculations have been carried out for four spin configurations referred to as the FM state (all spins of Ni, Co, Cr, Mn_Y, and Mn_Z are $\uparrow\uparrow$) and three ferrimagnetic states: FIM-I (spins of Cr on either the X, Y, or Z lattice are $\downarrow\downarrow$), FIM-II (spins of Mn_Z are $\downarrow\downarrow$), and FIM-III (spins of Mn_Z and Cr are $\downarrow\downarrow$). Second, the magnetic exchange parameters J_{ij} and electronic density of states (DOS) have been calculated using the equilibrium lattice parameters and magnetic reference states and the spin-polarized relativistic Korringa-Kohn-Rostoker (SPR-KKR) package [22] by employing the coherent potential approximation (CPA). The magnetic moments for Cr-doped $Ni_{45}Co_5Mn_{37}In_{13}$ obtained with the SPR-KKR package are listed in Ref. [17]. Finally, MC simulations of the Potts-BEG Hamiltonian model were carried out in order to extend the *ab initio* studies to finite temperatures using exchange couplings, magnetic moments, and anisotropy constants as input parameters. It is worth emphasizing that all technical details of *ab initio* and MC calculations are presented in Ref. [17].

The variation of total energy for different magnetic reference states of both 16-atom supercells is shown in Fig. 2(a). We note that the FM ground state of sample No. 1 has a lower energy than the FIM-I state of supercell No. 2, although the energy difference is small ($\approx$1 meV/f.u.). Therefore, the FM alignment is the stable magnetic ground state of austenite,

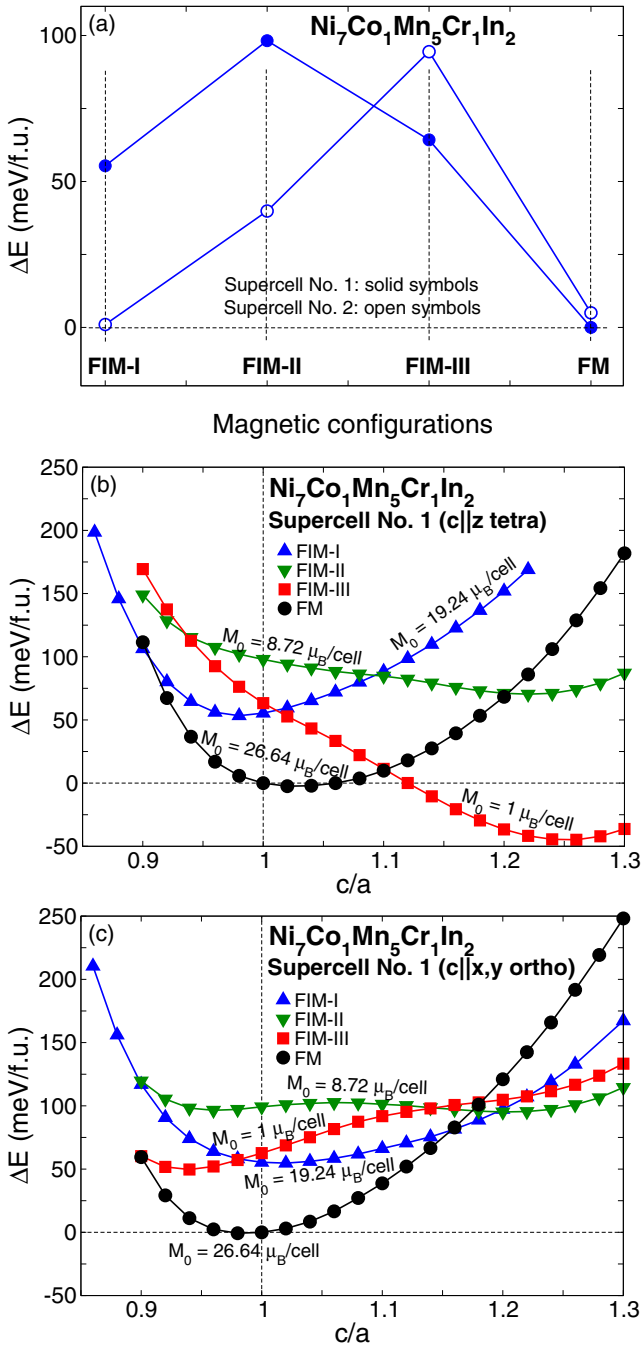

FIG. 2. (Color online) (a) The equilibrium total energies for different magnetic reference states for supercells No. 1 (open symbols) and No. 2 (solid symbols). (b), (c) Energies as functions of tetragonal ("tetra") and orthorhombic ("ortho") distortions for cell No. 1.

and in the following only results for supercell No. 1 will be presented. In order to investigate the trend for martensitic deformation, we have performed c/a calculations for tetragonal and orthorhombic distortions of supercell No. 1 along the z and y axes, which are presented in Figs. 2(b) and 2(c). Note that energies of the FM, FIM-I, and FIM-II configurations show approximately similar behavior for different distortions while a considerable difference in energy is found for the FIM-III configuration. On the one hand, when the distortion is

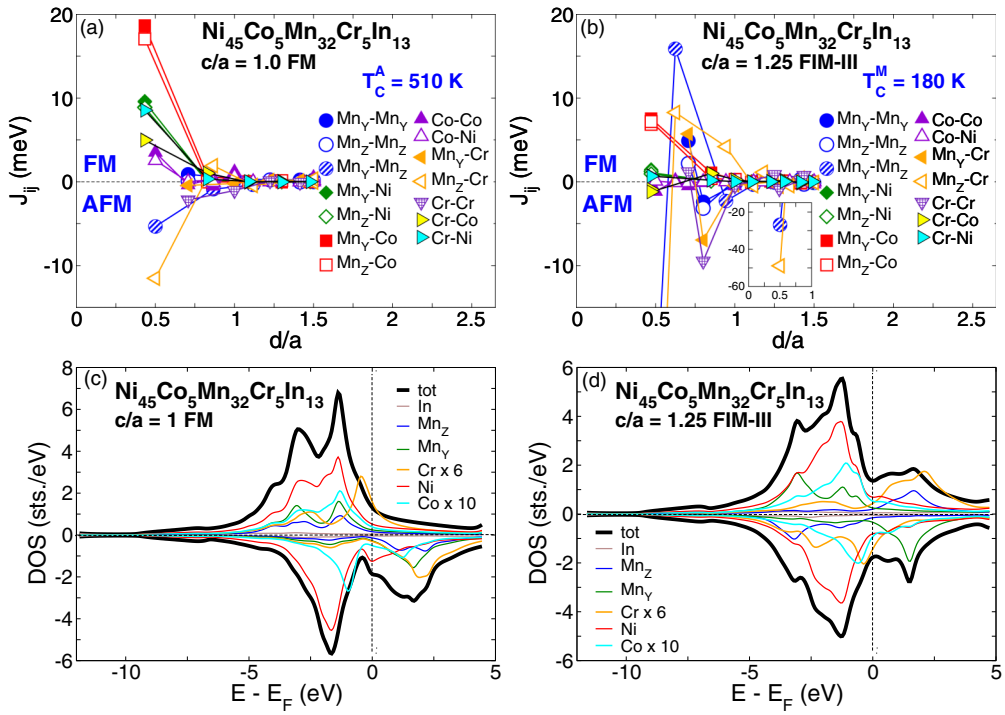

FIG. 3. (Color online) (a), (b) Calculated magnetic exchange couplings and (c), (d) element resolved DOS of $Ni_{45}Co_5Mn_{32}Cr_5In_{13}$ for the FM ($c/a = 1$) cubic phase and FIM-III ($c/a = 1.25$) tetragonal phase. T_C^A and T_C^M mark the Curie temperatures of austenite and martensite obtained from MC simulations.

performed along the z axis, the martensitic phase with the FIM-III configuration is achieved for a tetragonal ratio $c/a = 1.25$ while the remaining orders are not favorable in martensite. On the other hand, for orthorhombic deformation along the y axis, the FM martensitic phase is achieved for $c/a = 0.97$. This is related to two crystallographic inequivalent directions appearing in the supercell. Such subtle changes of energy on the atomic positions and spin configurations due to chemical disorder may favor strain glass trends [23].

Figures 3(a) and 3(b) show the coupling constants J_{ij} of the FM austenitic and FIM-III martensite structures of $Ni_{45}Co_5Mn_{32}Cr_5In_{13}$. In both cases the intersublattice interactions [$Mn_{Y(Z)}$-Co, $Mn_{Y(Z)}$-Ni, $Mn_{Y(Z)}$-$Mn_{Z(Y)}$, $Mn_{Y(Z)}$-Cr, and Cr-Co] provide the largest contribution to the exchange due to shorter distances compared to the intrasublattice interactions [$Mn_{Y(Z)}$-$Mn_{Y(Z)}$, Co-Co, Ni-Ni, and Cr-Cr]. We also notice that the Mn_Y-Mn_Z and $Mn_{Y(Z)}$-Cr exchange interactions in the first shell are five times larger in martensite than in austenite. It is obvious from Fig. 3(b) that the $Mn_{Y(Z)}$-Co exchange interactions are reduced by a factor of 2, while $Mn_{Y(Z)}$-Ni, Cr-Co(Ni), and Co-Co(Ni) coupling constants are close to zero. Large AFM (FM) exchange interactions between $Mn_{Y(Z)}$-Cr and $Mn_{Y(Z)}$-$Mn_{Z(Y)}$, in combination with smaller (larger) FM $Mn_{Y(Z)}$-Ni(Co), and Co-Co(Cr) interactions, will yield a lower (higher) Curie temperature of martensite (austenite), respectively. This may lead to the appearance of a PM gap between magnetically weak martensite and FM austenite. Hence, a sharp drop in magnetization is expected to occur across the martensitic transformation from austenite to martensite upon cooling. The calculated total and partial DOS of FM austenite and FIM-III martensite are shown in Figs. 3(c) and 3(d). The antibonding parts of the DOS around the Fermi level E_F mostly have contributions from Mn_Y and Mn_Z $3d$ states, while bonding parts and nonbonding parts for austenite (martensite) have Mn_Y, Mn_Z, and Ni $3d$ (Mn_Y and Ni $3d$) contributions, respectively. The difference in contributions to the bonding and nonbonding parts for austenite and martensite is associated with the reversed magnetic moment of Mn_Z and Cr in martensite compared to its parallel alignment in austenite. Since the concentration of Cr and Co atoms is small, they contribute little to the total DOS. The formation of a tiny pseudogap in both spin channels at E_F in Fig. 3(d) may help to stabilize the martensitic phase.

The interesting question is in how far the magnetocaloric properties of $Ni_{45}Co_5Mn_{37}In_{13}$ change when 5 at. % of Mn_Y is replaced by Cr. To answer this, we simulated the temperature dependence of the MCE properties shown in Fig. 4 using the Potts-BEG model and *ab initio* input parameters. As mentioned above, Cr and Mn_Z magnetic moments are antiparallel to the Mn_Y moment in martensite with $c/a = 1.25$ and they change their orientation in austenite. Therefore, an increase in both quantities, the total magnetization [Fig. 4(a)] and MCE [Figs. 4(c) and 4(d), is found at the martensitic transformation. Note that the MCE characteristics were numerically calculated from specific heat curves shown in Fig. 4(b). In order to determine the influence of Cr on the MCE of Co-doped Ni-Mn-In alloys, we also present in Figs. 4(c) and 4(d) the theoretical ΔS_{mag} and ΔT_{ad} curves in combination with the experimental behavior of ΔT_{ad} for $Ni_{45}Co_5Mn_{32}Cr_5In_{13}$, which has been taken from Ref. [8]. As shown, the addition

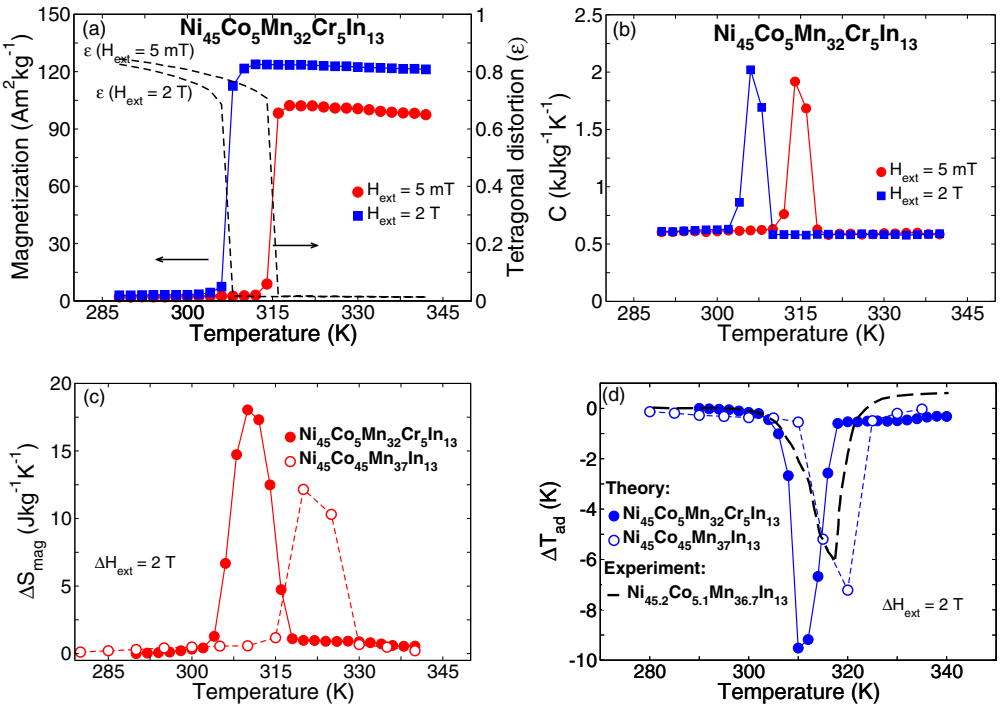

FIG. 4. (Color online) (a), (b) Magnetization and strain order parameters as well as total specific heat of $Ni_{45}Co_5Mn_{32}Cr_5In_{13}$ as a function of temperature for fields of 5 mT and 2 T. (c), (d) Magnetocaloric properties, ΔS_{mag} and ΔT_{ad}, of $Ni_{45}Co_5Mn_{32}Cr_5In_{13}$ for $\Delta H = 2$ T. The theoretical MCE for $Ni_{45}Co_5Mn_{37}In_{13}$ has been taken from Ref. [18]. The experimental value of ΔT_{ad} for $Ni_{45.2}Co_{5.1}Mn_{36.7}In_{13}$ for $\Delta H = 1.9$ T is shown by the dashed line [8]. All theoretical curves show only results for increasing temperature.

of Cr to Ni-Co-Mn-In leads to a large inverse MCE with $\Delta T_{ad} \approx -10$ K under a field change of 2 T, assuming the optimal spin configuration (FIM-III) in martensite.

Figure 5 shows that large individual spin moments of the transition elements of the Heusler alloys acting together in appropriate parallel spin configurations, which undergo a common spin-flip transition from FM austenite to FIM-II or FIM-III martensite, finally lead to a large jump of magnetization in favor of a large MCE for NiCoMnIn, NiCoMnAl, and NiCoMnCrIn. With an increase of Mn_Z atoms, the total magnetic moment of austenite increases while it decreases in martensite where the Mn_Y-Mn_Z exchange interaction is found to increase. Using rare earth elements such as Gd (which has the largest spin moment among all elements) as dopants instead of Cr may also act in favor of a large MCE. However, no large amounts of Gd can be dissolved in the Heusler alloys.

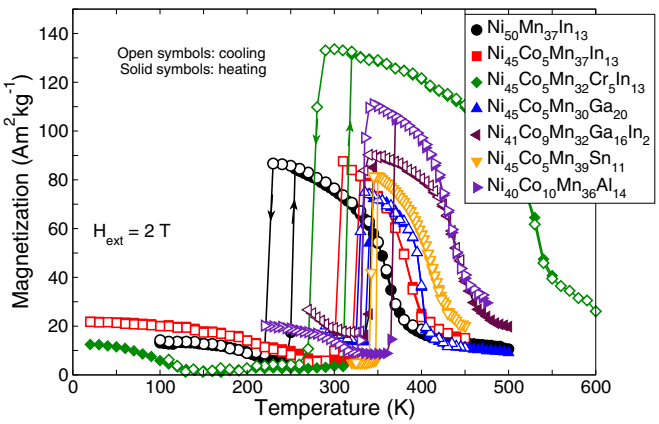

FIG. 5. (Color online) Heating and cooling magnetization curves across the first-order magnetostructural transition of NiMnIn, NiCoMnIn, NiCoMnCrIn, NiCoMnGa, NiCoMnGaIn, NiCoMnSn, and NiCoMnAl alloys in a field of 2 T.

For practical applications of the MCE, the refrigeration capacity (RC) is important. Note that the largest value of RC (~500 J/kg for $Gd_5Si_2Ge_2$) was obtained under ΔH of 5 T [2]. For 2 T, this drops to 120 J/kg [2], which becomes comparable to experimental and our theoretical RC value for $Ni_{45}Co_5Mn_{37}In_{13}$ [8,18] (see Table I). Compare also the RC values for the most studied MCE materials in Ref. [24].

In summary, we have combined *ab initio* calculations with MC simulations to study the influence of 5 at. % Cr on the MCE of $Ni_{45}Co_5Mn_{37}In_{13}$. The energy calculations have been carried out by using two kinds of 16-atom supercells of $Ni_7Co_1Mn_6In_2$ with different distributions of Mn_Z and

TABLE I. Experimental and theoretical magnetocaloric quantities of materials with magnetostructural transition. Here, the RC value is defined as RC $\approx -\Delta S \delta T$, where $\delta T = T_2 - T_1$ is the full width at half maximum of ΔS.

Compound	ΔS (J/kg K)	ΔH (T)	δT (K)	RC (J/kg)	ΔT_{ad} (K)
$Gd_5Ge_2Si_2$ (expt.) [2,3]	−14	2	8.5	120	7
$Ni_{45}Co_5Mn_{37}In_{13}$ (expt.) [8]	−18	1.9	6.5	−117	−6.2
$Ni_{45}Co_5Mn_{37}In_{13}$ (MC) [18]	−12	2	10	−120	−6.8
$Ni_{45}Co_5Mn_{32}Cr_5In_{13}$ (MC)	−18	2	8.3	−150	−10.0

In atoms on the In sublattice. We found that in the case of supercell No. 1, FM austenite with a large magnetic moment and FIM-III martensite with a small magnetic moment are energetically favorable compared to supercell No. 2. As a consequence, the drop in magnetization, the PM gap, as well as a large inverse MCE are obtained across the martensitic transformation between FM austenite and PM martensite upon cooling. The MCE results for the sample with supercell No. 2 are not shown here. They are less favorable than the MCE results for sample No. 1 because the equilibrium spin order for both austenite and martensite was found to be of FIM-I order. Hence, the magnetic moments of both phases are comparable and there will not be a large change in magnetization across T_m. This shows again how subtly the MCE reacts to defects, spin configurations, etc. Calculations for larger supercells and more different spin configurations would be needed in order to gain insight into the effects of atomic disorder. Note that the synthesizing of Heusler alloys with a high (low) magnetic moment in austenite (martensite) is the key to resolving the problem of MCE optimization. Finally, the hysteresis issue still needs to be considered, but this is beyond the scope of the current Rapid Communication. It was pointed out in Ref. [8] that pressure may help to considerably reduce the thermal hysteresis in the NiCoMnIn alloys or appropriate doping, which is under current investigation.

This work is supported by RFBR No. 14-02-01085, RSF-Russian Science Foundation No. 14-12-00570/14, and Ministry of Education and Science RF No. 3.2021.2014/K. P.E. thanks the DGF for funding (SPP 1599) and Prof. I. Karaman, Prof. R. Arróyave, and Dr. N. Singh for discussions.

[1] S. A. Nikitin, G. Myalikgulyev, A. M. Tishin, M. P. Annaorazov, K. A. Asatryan, and A. L. Tyurin, Phys. Lett. A **148**, 363 (1990).
[2] V. K. Pecharsky and K. A. Gschneidner, Jr., Phys. Rev. Lett. **78**, 4494 (1997).
[3] K. A. Gschneidner, Jr., V. K. Pecharsky, and A. O. Tsokol, Rep. Prog. Phys. **68**, 1479 (2005).
[4] A. Fujita, S. Fujieda, Y. Hasegawa, and K. Fukamichi, Phys. Rev. B **67**, 104416 (2003).
[5] K. G. Sandeman, Scr. Mater. **67**, 566 (2012).
[6] S. B. Roy, in *Handbook of Magnetic Materials*, edited by K. H. J. Buschow (Elsevier, Amsterdam, 2014), Vol. 22, p. 203.
[7] D. Y. Cong, S. Roth, and L. Shultz, Acta Mater. **60**, 5335 (2012).
[8] J. Liu, T. Gottshall, K. Skokov, J. D. Moore, and O. Gutfleisch, Nat. Mater. **11**, 620 (2012).
[9] C. Jing, X. L. Wang, P. Liao, Z. Li, Y. J. Yang, B. J. Kang, D. M. Deng, S. X. Cao, J. C. Zhang, and J. Zhu, J. Appl. Phys. **114**, 063907 (2013).
[10] S. Fabbrici, G. Porcari, F. Cugini, M. Solzi, J. Kamarad, Z. Arnold, R. Cabassi, and F. Albertini, Entropy **16**, 2204 (2014).
[11] V. K. Sharma, M. K. Chattopadhyay, L. S. Sharath Chandra, and S. B. Roy, J. Phys. D: Appl. Phys. **44**, 145002 (2011).
[12] V. K. Sharma, M. K. Chattopadhyay, L. S. Sharath Chandra, A. Khandelwal, R. K. Meena, and S. B. Roy, Eur. Phys. J.: Appl. Phys. **62**, 30601 (2013).
[13] V. Sánchez-Alarcos, V. Recarte, J. I. Pérez-Landazábal, J. R. Chapelon, and J. A. Rodríguez-Velamazán, J. Phys. D: Appl. Phys. **44**, 395001 (2011).
[14] M. Khan, J. Jung, S. S. Stoyko, A. Mar, A. Quetz, T. Samanta, I. Dubenko, N. Ali, S. Stadler, and K. H. Chow, Appl. Phys. Lett. **100**, 172403 (2012).
[15] M. Khan, I. Dubenko, S. Stadler, J. Jung, S. S. Stoyko, A. Mar, A. Quetz, T. Samanta, N. Ali, and K. H. Chow, Appl. Phys. Lett. **102**, 112402 (2013).
[16] T. Kihara, X. Xu, W. Ito, R. Kainuma, and M. Tokunaga, Phys. Rev. B **90**, 214409 (2014).
[17] See Supplemental Material at http://link.aps.org/supplemental/10.1103/PhysRevB.91.220409 for supporting information on first-principles and Monte Carlo details.
[18] D. Comtesse, M. E. Gruner, M. Ogura, V. V. Sokolovskiy, V. D. Buchelnikov, A. Grünebohm, R. Arróyave, N. Singh, T. Gottschall, O. Gutfleisch, V. A. Chernenko, F. Albertini, S. Fähler, and P. Entel, Phys. Rev. B **89**, 184403 (2014).
[19] V. V. Sokolovskiy, O. O. Pavlukhina, V. D. Buchelnikov, and P. Entel, J. Phys. D: Appl. Phys. **47**, 425002 (2014).
[20] G. Kresse and J. Furthmüller, Phys. Rev. B **54**, 11169 (1996).
[21] QUANTUM ESPRESSO package version 5.02 at http://www.pwscf.org.
[22] H. Ebert, D. Ködderitzsch, and J. Minár, Rep. Prog. Phys. **74**, 096501 (2011).
[23] Y. Wang, C. Huang, J. Gso, S. Yang, X. Ding, X. Song, and X. Ren, Appl. Phys. Lett. **101**, 101913 (2012).
[24] L. Huang, D. Y. Cong, H. L. Suo, and Y. D. Wang, Appl. Phys. Lett. **104**, 132407 (2014).